Novel Techniques for Slurry Bubble Column Hydrodynamics

First Annual Report for Grant DOE-FG 22-95 PC 95212

July 1, 1996

Section III: REPORT FROM WASHINGTON UNIVERSITY

M. P. Duduković, M. Al-Dahhan, J. Chen
S. Degaleesan, P. Gupta, S. Kumar, S. Roy

Chemical Reaction Engineering Laboratory
Department of Chemical Engineering
Washington University
Campus Box 1198, One Brookings Drive
St. Louis, MO 63130-4899

1 Introduction

The main goal of the study c conducted at the Chemical Reaction Engineering Laboratory (CREL) at Washington Univwersity as part of this DOE grant is to improve the basis of scale-up and operation of slurrrry bubble column reactors (SBCR) by an increased reliance on phenomenologically or fundammentally based hydrodynamic models which are experimentally verified.

For the first year the envisisioned objectives were :

- Complete the improvemments in Computer Automated Radioactive Particle Tracking and Computed Tomogra aphy (CARPT/CT), and develop the Monte Carlo based calibration for the CARPT technique.

- Complete studies with a air-water in a single diameter column and compare the results for velocity obtained by CARPT to those obtained by other techniques such as thermal probe and Particle Imagge velocimetry (PIV).

Improvements in CARPT technique encompasses two tasks. The first one involves the development of a filtering procedure to eliminate the fluctuating effects of the statistical nature of the emissions from the tracer particle. Although the mean quantities estimated from the CARPT measuremeents are unaffected by the fluctuations, accurate estimation of the turbulence and backmixiring parameters requires that the intrinsic noise caused by the fluctuations in emissions from the tracer be removed by some filtering procedure.

The other improvement in the CARPT technique is associated with the calibration procedure required for locating the particle position from the intensity of radiation measured by several detectors. In the current calibration procedure it is necessary to position the tracer particle at a few hundreed known locations inside the reactor and acquire the intensity data from several detectors strategically positioned around the reactor. These measurements are then used to develop an intensity versus distance relationship for all the detectors used. This is an extremely laborious s process and often difficult to perform in reactors with opaque walls. Moreover, the calibration needs to be done in-situ. In addition, the accuracy of the calibration and the subsequent location of the tracer depends on the accuracy of positioning of the tracer at a given location. In order to avoid this extensive and cumbersome calibration process one of the objectitives is to develop a phenomenological approach to account for geometry and the attenuation properties of the flowing phases on the radiation measurement process. The modeling of the emission of radiation, the attenuation by the flowing phases as well as the column wall and the subsequent detection by the scintillation detectors is accomplished by the Monte Carlo method.

In this report we first presesent a brief account of the progress made in each of the above mentioned research areas.

2 Filtering CARPT Data Using Wavelet Based Technique

Owing to the quantized naturere of the γ photons, the intensity of radiation exhibits continuous fluctuations in time. The e emission of γ rays follows a Gaussian distribution (with mean, n_c, and standard deviation, $\sqrt{\sqrt{n_c}}$). This is manifested as white noise in the data and results in the generation of "spuriousis velocities", i.e., non-zero velocities for a physically stationary particle. Consequently, thhe instantaneous velocities measured have partial contribution from the fluctuations in the scsource particle emission. Time (ensemble) averaging of the instantaneous velocities in eachh compartment eliminates these source fluctuations (since the fluctuations have a Gaussian ddistribution with zero mean). This is reflected in the negligible mean spurious velocities calcuulated, which are in the order of 0.1 cm/sec (For comparison, the actual monitored velocitiesss are 10 cm/sec to 50 cm/sec). However, the fluctuating velocities and root mean square fluuctuating velocities measured, are resultant of the fluctuations due to the turbulent flow fieldd and the spurious velocities. This causes an over-estimation of the turbulence quantities that t are measured. Therefore it is necessary to eliminate or reduce to the best possible extent, thhe spurious fluctuations in the particle position data in order to obtain more accurate estimnates of the turbulence parameters.

2.1 Objectives

Since the tracer particle is ofof finite size ($\sim 2mm$), it follows eddies only up to a certain frequency range correspondingg to the length scale of the size of the particle. An estimate of this frequency limit can be e calculated on the basis of single phase flow turbulence theory (Hinze 1959). It is found too be in the range $10 - 35$ Hz, depending on the mean flow conditions, which vary within a the column.

Fourier domain filtering waas first attempted using a third order low pass Butterworth filter with a cut-off frequency of 100 Hz. It can be observed from Figure 1a (note the highlighted regions enclosed in boxes) thaat the resulting filtered signal is unable to capture the sharp peaks present in the original s signal. As a result, these sharp changes that characterize the flow are removed as noise, as c can be seen in the bottom part of Figure 1a. This shows strong peaks in the filtered noise whhich are not characteristic of the white noise that is known to cloud the data. If the cut-offff frequency for the filter is increased, this results in residual

high frequency components of f the white noise in the signal. This problem arises due to the inherent non-stationary nature e of the signal obtained from CARPT measurements describing the turbulence in the system, ; which has localized frequency characteristics. This renders a low pass filter unsuitable for fifiltering CARPT data.

Wavelet analysis, which is s a time-frequency based method is a suitable alternative and has the distinct advantage ovver Fourier transform techniques, as it can be used to analyze non-stationary data. This is illllustrated in Figure 1b where the filtered noise, using a wavelet based technique resembles the e white noise present in the intensity data.

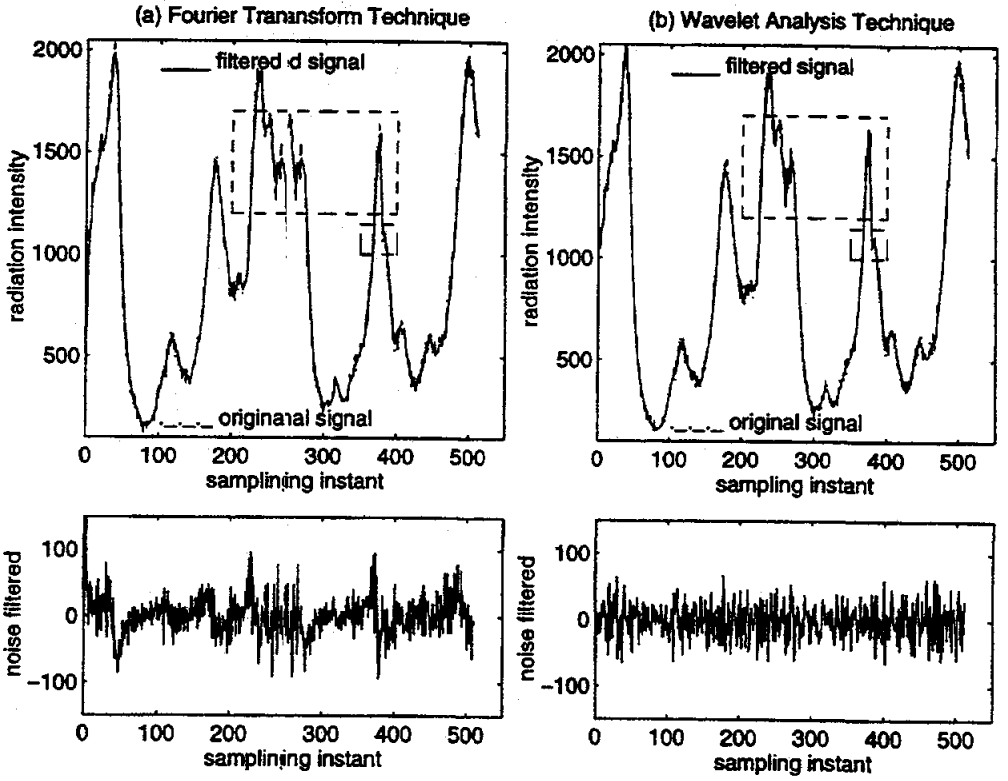

Figure 1: Comparison of Fouririer Transform and Wavelet Analysis Techniques for Filtering CARPT Data

The objective of this work i is to apply the wavelet packet algorithm for filtering CARPT data. To demonstrate its suiiitability in this regard, an experiment is conducted with a controlled motion of the radioactive tracer particle. This enables *a priori* knowledge of the trajectory of the particle and l provides a reference against which the results from CARPT experiments subject to wavelelet packet filtering can be compared. A quantitative estimate of the errors involved in the e estimation of the particle position, as well as the extent to which the intrinsic noise in the data is removed can therefore be arrived at. Thereafter the technique is applied to data frrom bubble column experiments.

2.2 Wavelet Analysis

The wavelet transform of a signal refers to the projection of the signal onto local, re-scalable functions called wavelets. These functions have prescribed smoothness, are well localized in time and frequency and form a well-behaved basis (Daubechies 1988). Wavelets, $\psi_{a,b}(t)$, of constant shape are generated by the dilation and translation of a prototype or mother wavelet $\psi(t)$. Therefore each wavelet has a specific time-frequency localization. Wavelets of high frequency are narrow (well localized) in time, while wavelets of low frequency are broad in time. As a result wavelets are able to capture both short lived high frequency phenomena as well as longlived low frequency phenomena. This enables them to work well for filtering non-stationary signals clouded with white noise.

In what follows we focus on those aspects of wavelet analysis that are used in this work, introducing with the underlying basic concepts, discrete wavelet transforms (DWT) and wavelet packet decomposition (WPD). DWT involve the projection of a data set, $f(t)$, onto discrete wavelets to give discrete wavelet coefficients. This is represented as :

$$\langle f, \psi\psi_{m,n} \rangle = 2^{-m/2} \int_{-\infty}^{\infty} f(t)\psi(2^{-m}t - n)dt \tag{1}$$

where m and n represent the discretized dilation and translation parameters respectively. DWT is a special case of wavelelet packet decomposition (WPD). In WPD, a library of wavelet packets are used, from which a a variety of bases can be extracted to represent the signal. The construction of wavelet packkets can be represented in a hierarchy as shown in Figure 2, where two filters, H, a low-ppass filter and G, a high-pass filter, are used to generate the entire library of wavelet packkets using a recursive scheme (Wickerhauser 1994). The nature of the wavelet packets generated depends on H and G. There are a variety of wavelets available, of which Daubechiess' (1988) orthonormal, compactly supported wavelets are most popular.

The decomposition of the signal onto these wavelet packets constitutes WPD. As in the case of DWT, the wavelet packket coefficients are given by :

$$\lambda_{s,f,p} = \langle f, \psi_{s,f,p} \rangle = 2^{-s/2} \int_{-\infty}^{\infty} f(t)\psi_f(p - 2^{-s}t)dt \tag{2}$$

where λ is the wavelet packet coefficient. The resulting library of wavelet packet coefficients contains redundant information, from which a best basis is chosen by minimizing the entropy of the coefficients (Coifman and Wickerhauser, 1992). The more the randomness in the signal, the greater its entropy, and therefore the greater the number of coefficients required to represent the signal accurately which means larger information cost.

White noise has very poor time-frequency localization, or in other words is incoherent.

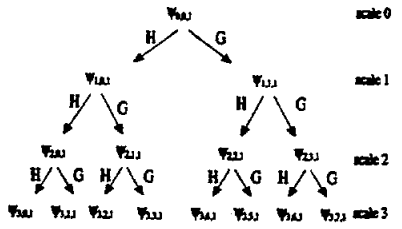

Figuure 2: Hierarchy of Wavelet Packets

Therefore, as mentioned abovee, a large number of wavelet packet coefficients are needed to represent it. We are interesteced in the application of the best basis algorithm in denoising noisy signals. The idea here is t to extract coherent parts present in the signal (signal features with good time-frequency localalization), using the Matching Pursuit Algorithm (Mallat and Zhong 1992). In the Matchingg Pursuit Algorithm the signal is decomposed into a coherent part and an incoherent part. The coherent part is extracted by retaining a fraction of the signal energy in the form of a fefew large wavelet packet coefficients. The remaining incoherent part is decomposed several timmes to extract all the coherent parts remaining in it. All the individual coherent parts, thusis extracted, are superimposed to give the filtered signal. The incoherent part remaining at tthe end is rejected as noise. The advantage of the algorithm is that exact characterization of t the process is not required. In the present work, we essentially adopt a modification of the maatching pursuit algorithm. If the signal to noise ratio is high, i.e., the energy level of the nnoise in the signal is low, a suitable threshold for the energy is set, by which a large numbeer of coefficients with the lowest energy, which are known to represent the randomness due t to the noise, are set to zero, thereby removing the noise.

2.3 Wavelet Packet Filtering of CARPT Experimental Data

The white noise present in thhe radiation intensity data, is transmitted to the estimated position of the particle in carteesian coordinates, $P(x, y, z)$. It is found that the noise in each coordinate is white noise uncoorrelated with each other. Filtering of the radiation intensity and subsequent estimation of t the particle positions yields results similar to those generated by direct filtering or denoisingg of the particle positions along each coordinate. The latter approach of filtering the positioion data is more efficient in both time and computing resources. Therefore the filtering methodd will be applied directly to the x, y, z position data.

Wavelet packet decompositition using Daubechies' orthonormal, nearly symmetric wavelets is employed for this analysis. TThe algorithm for analysis and filtering of the data is explained below. The original signal is dilivided into data sets of length $N = 2^L$; $L = 10$ to 13. Given a data set of length N samploled at constant frequency, the wavelet packet decomposition

and subsequently the best basis representation is obtained. The wavelet packet coefficients (wpc) in the chosen basis are arranged in descending order of energy (energy $E_{wpc} = wpc^2$), simultaneously keeping tag of the position of each coefficient. The first few significant coefficients correspond to the coherent part of the signal while the remaining weak coefficients depict the noise. The coherent part is extracted by retaining the first few largest wavelet packet coefficients that possess an energy ($E_\epsilon = \epsilon E_S = \sum_{i=1}^{I_\epsilon} wpc^2$) equivalent to a fraction ϵ of the total signal energy ($E_S = \sum_{i=1}^{N} wpc^2$). These coefficients are then re-ordered and reconstructed to yield the filtered signal. The weak coefficients (incoherent part) that remain are re-ordered and reconstructed to give the noise filtered. The tuning parameter in this algorithm is the energy threshold ϵ. This parameter is evaluated by conducting trial runs for a few data sets in the signal. The value of ϵ essentially depends on the results of calibration for a given experiment. This affects the magnitude of the spurious fluctuations in the position data, which is determined from the data for a stationary particle. Characteristics of white noise, such as the autocorrelation coefficient and power spectral density, are used as a check to select a proper threshold to ensure that no coherent part of the signal is removed. Experiments show that the energy threshold is generally around $95 - 98\%$ of the total signal energy. It is found that the results are insensitive to minor variations in the threshold value. Filtering using the above algorithm ensures maximum extent of reduction of the noise in the data, resulting in a smoother version of the signal and retains the sharp features arising from the nature of the flow in the system.

The algorithm is implemented using the mathematical package MATLAB. The wavelet toolbox[1] provides the necessary subroutines for construction of wavelets, WPD and reconstruction of the signal.

In order to verify the applicability and effectiveness of the algorithm for filtering noise from the data, we test the algorithm with data collected from experiments for a controlled motion of the tracer particle. .

2.4 Experimental Setup

The experimental setup consists of two motors, a screw conveyor and a plate as shown in Figure 3. Motor I is secured at the bottom of the structure and is geared to a screw conveyor that is positioned vertically. The screw conveyor supports a vertical frame on top of which the plate is mounted. The shaft of motor II, which is fixed to the top of the plate, is connected to a smooth, circular disc. The radioactive particle to be tracked is fixed to the tip of a thin plexiglas rod attached to the disc. Operation of motor II causes the particle to

[1] wavbox is the wavelet toolbox x written by Taswell for a MATLAB environment

move in a circular motion. Thee maximum frequency of motion is 3 Hz. The distance of the particle from the center of the e circle varies from 7 to 8 cm. Simultaneously motor I causes the plate held to the frame to o move vertically in "up and down" motion (with frequencies of the order of 0.1 Hz). The mnaximum vertical distance traversed by the particle is 6.4 cm. By this arrangement the partiticle is made to move in a spiraling 3D motion, with high (3 Hz) and low (0.2 Hz) frequencicies. The two motors are driven by microprocessors, which are interfaced with a personal commputer. This arrangement ensures the precision with which the particle moves. A trolley r system with guiding wheels provided for guiding the frame helps in minimizing the vibratation of the setup. The entire structure is supported on the plenum centered between the d detector supports (not shown in figure). Sixteen strategically positioned detectors are used f for detecting the γ radiation. Calibration is first done using various particle positions that c cover the entire range of experimental runs. Subsequently the experimental runs are performeed. In each run, the speed of the two motors is varied, thereby varying the velocity of the partrticle. Eight such runs are performed.

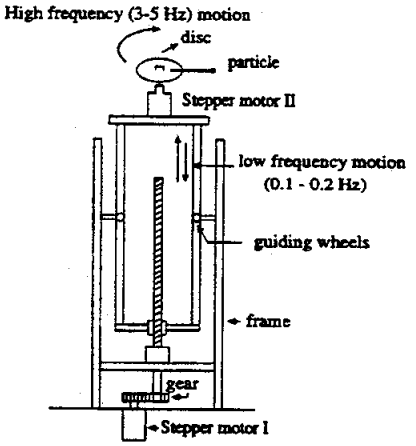

Figure 3: Experirimental Setup for Controlled Motion of Particle

2.5 Results and Disccussion

The details of the experimentatal runs carried out are shown in Table 1. Motor I moves the particle in a linear vertical mootion, i.e. along the z axis in cartesian coordinates. Motor II moves the particle in a horizonntal two dimensional circular trajectory, i.e. in a $x-y$ plane. A parametric representation ofbf the trajectory of the tracer particle is given as:

$$x_t = x_c + r_p cos(\theta_0 \frac{\pi}{180}) + r_p cos(2\pi\omega_2 t);\ \ y_t = y_c + r_p sin(\theta_0 \frac{\pi}{180.0}) + r_p sin(2\pi\omega_2 t);\ \ z_t = z_0 + \omega_1 t \quad (3)$$

where x_c and y_c are biasesss in position due to experimental constraints. r_p is the radius of curvature which the particlcle traverses. θ_0 is the initial angular position of the particle. ω_2 is the frequency of rotationn of motor I. ω_1 gives the displacement of the particle per unit time and is related to the rppm of motor I. Motor I is programmed to move 800 steps in the clockwise direction (125 ststeps in the clockwise direction is equivalent to 1 cm) and 800 steps in the counterclockwise e direction, repeating this periodic motion several times. This induces a frequency of about (0.1 Hz in the z direction of motion. Based on the trajectories, the existing Lagrangian velocicities v_{x_t}, v_{y_t} and v_{z_t} are calculated.

Tabble 1. Details of Experimental Runs

Run No.	$r_f r_p$ cmm	θ_0, deg	ω_1 cm/sec	z_0 cm	z_f cm	ω_2 1/sec
Run 1	6.9964	315	2.0	112.21	118.61	2.75
Run 2	6.9964	315	2.0	112.21	118.61	1.75
Run 3	7.1180	315	2.0	112.21	118.61	1.00
Run 4	7.1180	315	2.0	112.21	118.61	2.00
Run 5	7.1180	315	2.0	112.21	118.61	2.75
Run 6	7.9989	315	2.0	112.21	118.61	2.75
Run 7	7.9989	315	2.0	112.21	118.61	1.50
Run 8	7.9989	270	2.0	112.81	119.41	0.00

The instantaneous positioon data x_p, y_p and z_p resulting from CARPT experiments for the controlled motion of the ı particle are subject to wavelet packet filtering as discussed in the previous section, yielding g filtered results x_f, y_f and z_f. Thereby the particle velocities from CARPT measurements ((sampling frequency is 50 Hz) before filtering, v_{x_p}, v_{y_p} and v_{z_p}, and after filtering, v_{x_f}, v_{y_f} $v_{z_f z_f}$, are obtained.

The results are analysed b by comparing the magnitude of the error in positions and velocities in each direction. For r this purpose the root mean square (rms) error in position and velocity are used. Figure 4a s shows the actual trajectory y_t for a period of 10 secs, for Run 5 reported in Table 1. Figurere 4b is a comparison of the error in estimating the successive y positions of the particle. Fi'igure 5 show the velocity of the particle along the y axis with the errors before and after fifiltering. A summary of the results for the entire set of runs is presented in Table 2 whichh reports the errors in position x, y and z, and spurious rms velocities, before and after fifiltering. It is evident by examining the results, that there is significant improvement in thee accuracy of estimation of both the positions and velocities of

the moving particle. The resisidual error (spurious rms velocities) after filtering the data is 2-5 cm/sec. There is an averrage of 75% reduction in the level of noise in the data. With regard to the magnitude of thhe rms fluctuating velocities of the liquid in bubble columns, which are an order of magnituude higher, the reduction in error is considered substantial.

Table 2. Errors in Estinimation of Particle Position (cm) and Velocity (cm/sec)

		error in position, cm				error in velocity, cm/sec	
		Beforee Filtering		After Filtering		Before filtering	After Filtering
Run No.	Direction	rms	min/max	rms	min/max	rms	rms
Run 1	x	0.32	-1.17,1.12	0.19	-0.7,0.6	20.5	4.16
	y	0.36	-.15, 1.2	0.26	-0.75, 0.8	20.01	4.66
	z	0.49	-1.7,1.4	0.25	-0.7,0.74	30.36	1.68
Run 2	x	0.30	-1.23, 1.25	0.2	-0.76, 0.64	21.0	5.6
	y	0.33	-1.43, 1.34	0.22	-0.79, 0.86	19.4	5.7
	z	0.49	-1.6,1.6	0.2	-0.67,0.8	29.6	1.6
Run 3	x	0.32	-1.16,1.13	0.21	-0.7,0.9	19.3	3.2
	y	0.31	-1.2,1.2	0.21	-0.85,0.8	18.0	3.6
	z	0.47	-1.5, 1.75	0.17	-0.9, 0.6	28.9	1.34
Run 4	x	0.32	-1.08,1.12	0.22	-0.75,0.86	19.5	4.8
	y	0.32	-1.5,1.25	0.23	-0.7,0.75	19.0	4.5
	z	0.46	-1.4,1.4	0.21	-0.65,0.61	29.0	1.38
Run 5	x	0.3	-1.11,1.32	0.19	-0.9,0.66	20.2	5.4
	y	0.29	-0.89,0.9	0.16	-0.61,0.65	18.7	3.8
	z	0.47	-1.6,1.4	0.22	-0.87,0.72	29.2	1.56
Run 6	x	0.32	-1.36,1.08	0.19	-0.55,0.52	20.9	5.3
	y	0.29	-1.4,1.0	0.17	-0.68,0.7	19.11	3.4
	z	0.39	-1.42, 1.45	0.14	-0.64,0.32	26.1	1.01
Run 7	x	0.31	-1.16,1.08	0.21	-0.8,1.0	19.78	4.18
	y	0.28	-1.14,1.11	0.14	-0.84, 0.82	18.69	3.51
	z	0.37	-1.09,1.21	0.20	-0.86, 0.72	25.73	1.48
Run 8	x	0.31	-0.97,1.03	0.03	-0.04,0.03	16.99	0.07
	y	0.28	-1.10,1.15	0.007	-0.01, 0.02	17.94	0.04
	z	0.40	-1.3,1.03	0.25	-0.79, 0.5	24.29	1.05

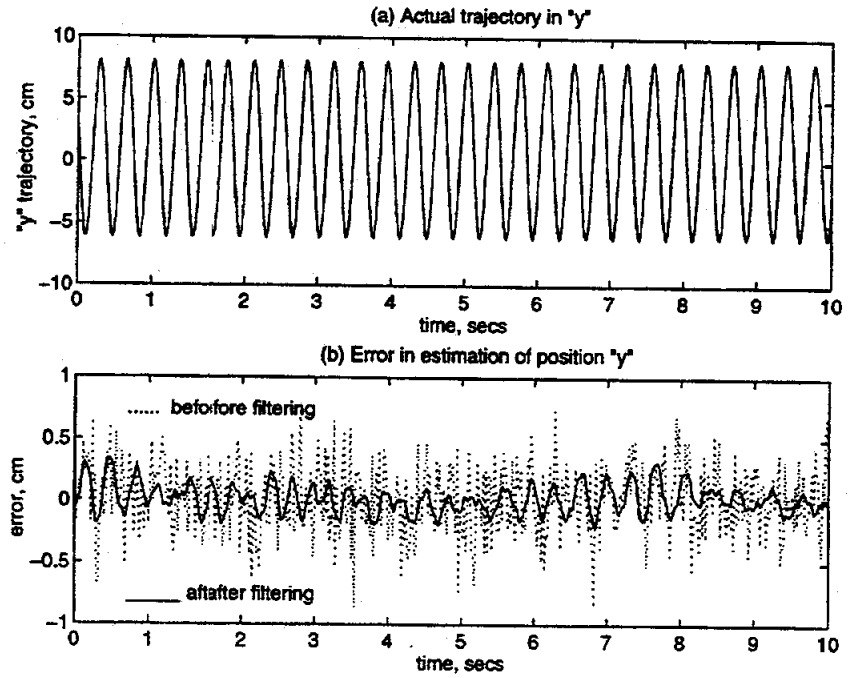

Figure 4: RResults for RUN 5 : Trajectory y of Particle

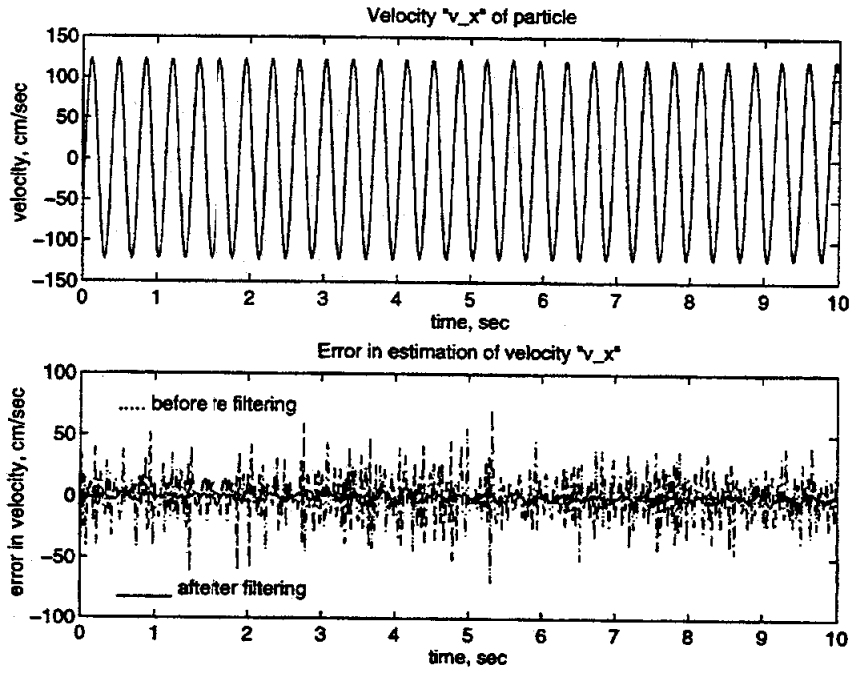

Figure 5: Results for RUN 5 : Velocity v_x and Error in Estimation of Velocity of Particle

The experiment for the conntrolled motion of the tracer particle thus provides a firm basis with which the effectiveness of the wavelet analysis technique for filtering the intrinsic noise in the instantaneous position d data is substantiated.

2.6 Results for a Buubble Column Experiment

We now show results for filteriring of the data from a bubble column experiment. The experimental conditions for the runn considered are : column diameter 19.05 cm, superficial gas velocity 4.0 cm/sec and superfifficial liquid velocity 0 cm/sec. The results presented in Figures 6 and 7 are one dimensional pprofiles generated by averaging over the middle section of the column, where the flow is fullly developed. As expected, there is no appreciable difference between the filtered and originnal mean axial velocity profiles shown in Figure 6. This is because time averaging of the instantaneous velocities, averages all the fluctuations in the data,

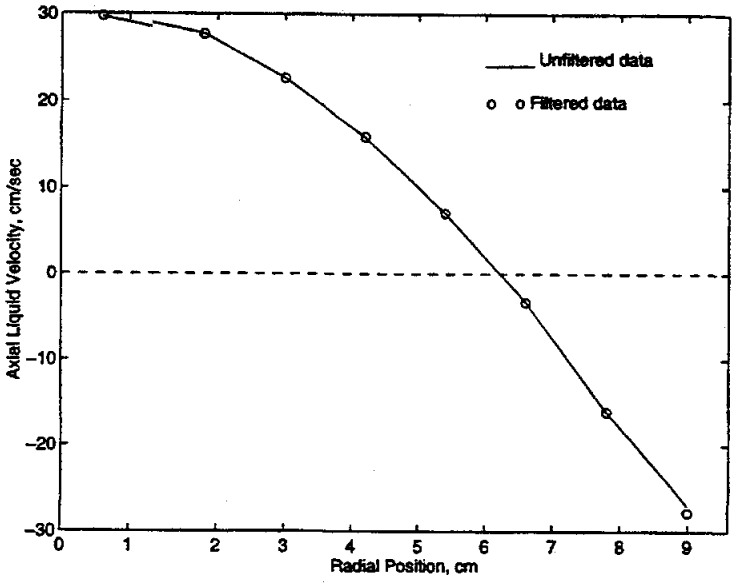

Figure 6: One Dimensional MMean Axial Liquid Velocity for an 8″ Column, U_G 4.0 cm/sec

including the inherent noise ddue to statistical fluctuations of the radiation. Figure 7 shows the turbulent kinetic energy. HHere it can be seen that filtering has reduced the magnitude of these parameters. The results from filtering experimental data are validated by comparing the Reynolds shear stress profiles obtained in a column of diameter 14 cm with results from Menzel et al. (1990) who usedd a hot wire anemometer to measure the instantaneous liquid velocities in a bubble column. . The results shown in Figure 8 suggest a good comparison for the Reynolds shear stress usinng the two techniques.

2.7 Conclusions

A wavelet packet based algorithm reduces the level of noise in the CARPT data. The algorithm is validated by designing and conducting a CARPT experiment with the controlled motion of the particle, whereby an *a priori* knowledge of the trajectory of the particle is

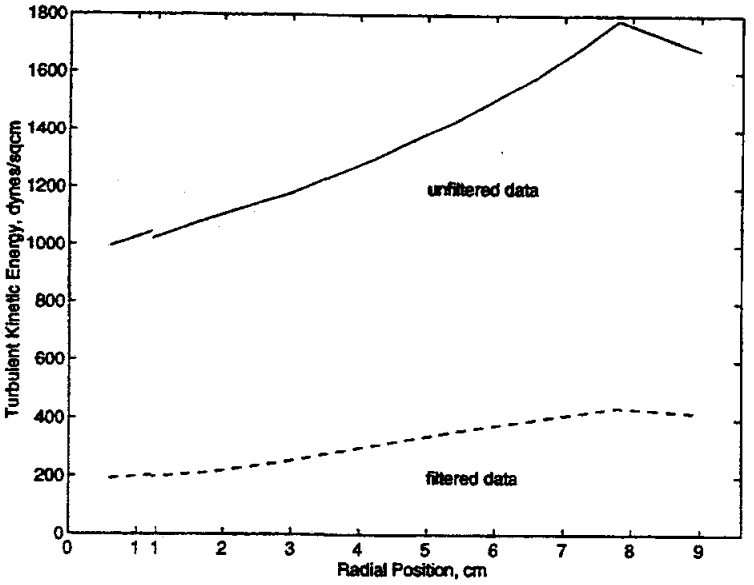

Figure 7: One Dimensional 1 Turbulent Kinetic Energy for an 8″ Column, U_G 4.0 cm/sec

possible. When applied to dalata for a bubble column experiment, substantial reduction in the noise is seen. This yields nmore accurate results for the turbulence parameters estimated, which is of importance in the ɜ modeling of bubble columns and other multiphase reactors.

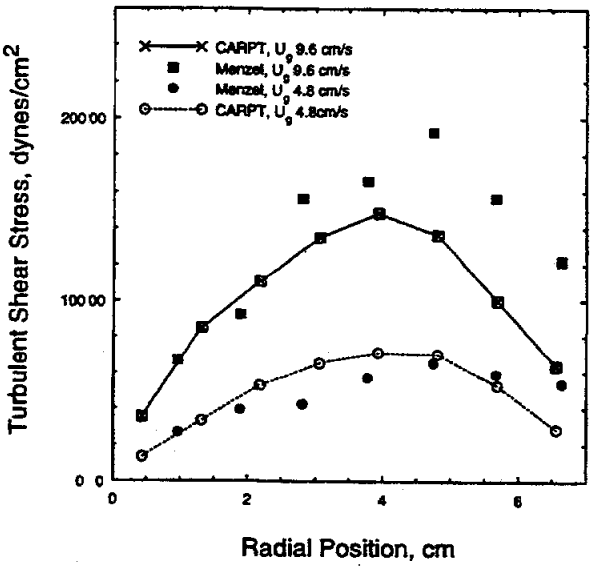

Figure 8: Comparison of Expperimental data for Turbulent Shear Stress from CARPT with Data of Menzel* (1990), Col. : Dia 14 cm

3 Monte Carlo SSimulation of the Radiation Measurement Process

The specific objectives for thisis part of the research is as follows :

1. To develop an efficient MMonte Carlo simulation program for calculating the efficiency of a cylindrical NaI detetector receiving radiation emitted from a point source located at an arbitrary positionn inside the reactor with or without internals. This would basically eliminate the t time-consuming in-situ calibration procedure in utilizing the Computer Automated RRadioactive Particle Tracking (CARPT) facility to study the flow pattern/mixing meechanism in multiphase reactors.

2. To determine the dynamnic location of a radioactive particle by using the 3-D position-counts maps for all detetectors obtained by using the Monte Carlo simulation. This would improve the accurracy for locating the particle position from count data received by each detector, since 3-D mapping is used instead of 1-D mapping adopted by the in-situ calibration processss.

3. Verify the Monte Carloo simulation by comparing the calculated counts with those measured at a number oof known locations inside the reactor. Optimize the dead-time constant of detectors anod the linear attenuation coefficient of reactor media to best fit the experimental and thheoretical data.

4. Write a program to deterermine the particle location from the count data on all detectors and the position-counts maps obtained from the Monte Carlo simulation.

5. Verify the accuracy of tthe program by comparing the predicted particle position and its actual position by plalacing the radioactive particle into several known location.

Progress has been made inn developing a Monte Carlo simulation program for calculating the detector solid angle, totall efficiency and photo-peak efficiency. The tracer particle and detector can be at any positioon (particle inside reactor, and detector outside reactor). The distances travelled by the phottons from the tracer inside the reactor and through reactor wall are calculated exactly. The alabsorption of γ-ray by the reactor media and reactor wall are also considered. The simulateed results by this program are compared with other simulated results reported in literature a and the comparisons are good.

The approach adopted for t the Monte Carlo simulation is described in the paper by Beam et al. (1978). Some modificcations and additions were made to account for the photons absorbed by the flowing phasses in the reactor and by the reactor wall. Randomly chosen

γ-rays emitted within the detetector solid angle (Ω) was employed by Beam et al. (1978) and Larachi (1994) to calculalate the detector efficiencies. In order to obtain an accurate simulation, a large number oof γ-rays (more than 4000) within the solid angle has to be calculated. To increase the acccuracy and simulation speed, Gaussian quadrature, instead of randomly picked γ-ray withinn the solid angle, is applied to perform the multi-dimensional integration. It is shown that : the results from the Monte Carlo simulation is accurate with 30 Gaussian points in one angular direction, i.e. total of 900 points for the surface integral.

3.1 Approach for MMonte Carlo Simulation

In the following we briefly ssummarize the steps involved in computing the detector efficiencies. To calculate the deletector efficiencies by the Monte carlo method, the following parameters need to be determmined.

1. The solid angle Ω subteended by the detector surface as seen from the tracer particle position;

2. The probability of non-iinteraction f_a of γ-rays emitted within Ω with the reactor media (gas-solid mixture) and l reactor wall, which is calculated by:

$$f_a(\alpha,\theta) = \exp\left[-\sum_{i=1}^{n}\mu_i d_i(\alpha,\theta)\right] \tag{4}$$

where μ_i is the total linnear attenuation coefficient of the material i in the γ-ray path, and d_i is the distance itit travels in the direction of (α, θ), α is the angle with the line normal to the detector : axis, θ is the angle with the detector axis. The geometry is illustrated in Fig. 9. TThe detector axis is normal to the detector front face, with the origin at the center of ddetector face.

3. The probability of interaraction f_d of γ-ray with the detector crystal. For total efficiency

$$f_d(\alpha,\theta) = 1 - \exp\left[-\mu_d d(\alpha,\theta)\right] \tag{5}$$

where μ_d is the total attttenuation coefficient of detector crystal and d is the distance of γ-ray travelled in the deletector by an undisturbed γ-ray along the direction of (α, θ).

4. For photo-peak efficiencacy, the calculation is more complicated since the Compton interaction has to be conmsidered, the probability of photo-peak interaction f_p can be

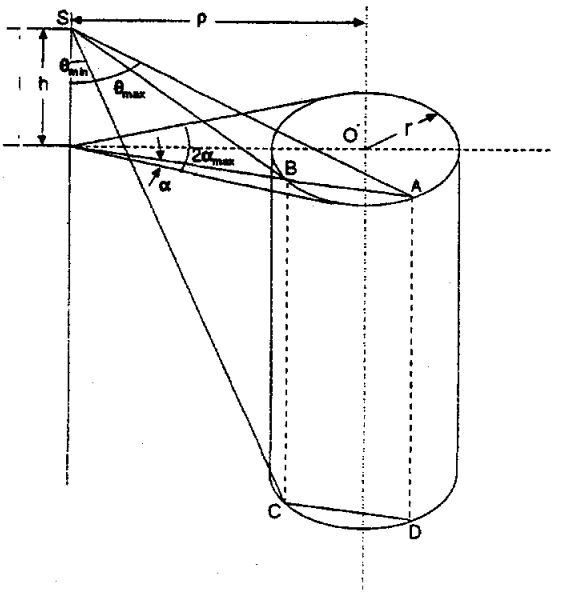

Figure 9: Angles s and Distances Used in Monte Carlo Simulation

written as:

$$
\begin{aligned}
f_p &= w_1 \frac{\tau_1}{\mu_1} + w_\nu \frac{\tau_\nu}{\mu_\nu} \prod_{j=2}^{\nu} w_{j-1} \frac{\sigma_{j-1}}{\mu_{j-1}} \\
w_j &= 1 - \exp\left[-\mu_j d_{eff}\right]
\end{aligned}
\tag{6}
$$

where w_1 is equal to f_d irin eq.(2), d_{eff} is the effective distance of γ-ray travelled, τ_j, σ_j and μ_j is the photoelectriric, Compton and total attenuation coefficients ($\mu_j = \tau_j + \sigma + j$), respectively. It should beoe mentioned that τ_j, σ_j and μ_j are a function of γ-ray energy. After each Compton intereraction, the γ-ray (photon) energy and direction changes. The distance travelled in the e new direction is randomly distributed between zero and the maximum distance it maay travel inside detector crystal in the new direction.

The total efficiency ϵ and pphoto-peak efficiency P_ϵ can be calculated by:

$$
\epsilon = \iint_{\Omega} \frac{\vec{r}.\vec{n}}{r^3} f_a(\alpha,\theta) f_d(\alpha,\theta) ds \tag{7}
$$

$$
FP_\epsilon = \iint_{\Omega} \frac{\vec{r}.\vec{n}}{r^3} f_a(\alpha,\theta) f_p(\alpha,\theta) ds \tag{8}
$$

where $\vec{r}$ is the vector from poirint source to a variable point p on the exposed detector surface, $\vec{n}$ is an external unit vector loocally normal to the surface at p, and ds is the area around p.

According to Beam et al. (:(1978) an appropriate statistical weight $w(\alpha, \theta)$ can be assigned to each sample direction (α, θ). If N randomly chosen γ-rays are sampled in the tracer-detector solid angle Ω, the soolid angle, total and photo-peak efficiencies can be evaluated by:

$$\Omega := \frac{4\pi}{N}\sum_{i=1}^{N} w(\alpha_i, \theta_i) \tag{9}$$

$$\epsilon := \frac{1}{N}\sum_{i=1}^{N} w(\alpha_i, \theta_i) f_a(\alpha_i, \theta_i) f_d(\alpha_i, \theta_i) \tag{10}$$

$$P_\epsilon := \frac{1}{N}\sum_{i=1}^{N} w(\alpha_i, \theta_i) f_a(\alpha_i, \theta_i) f_p(\alpha_i, \theta_i) \tag{11}$$

The angle α_i and θ_i is determiiined by the tracer position and the point where γ-ray i entered the detector. In order to obtaain accuracy values of ϵ and P_ϵ, a large number of N (5000 to 10000) is required since they ; are randomly selected. However, we can apply the Gaussian quadrature to efficiently perfoform the surface integration. It will be shown later that with $n = 30$ Gaussian points in onne angular direction (total number of γ-rays sampled equals to 900 in two angular directicions), the simulation results are comparable with those from randomly selected 5000 pointits. Actually, if one only wants to calculate the solid angle and total efficiency, 15 ($n = 1$ 15) Gaussian points in one angular direction are sufficient to obtain accurate values. The eequations for calculating the solid angle, total and photo-peak efficiencies using Gaussian quaadrature become:

$$\Omega = \pi \sum_{i=i=1}^{n}\sum_{j=1}^{n} w_g(i) w_g(j) w(\alpha_i, \theta_j) \tag{12}$$

$$\epsilon = \frac{1}{4}\sum_{i=i=1}^{n}\sum_{j=1}^{n} w_g(i) w_g(j) w(\alpha_i, \theta_j) f_a(\alpha_i, \theta_j) f_d(\alpha_i, \theta_j) \tag{13}$$

$$P_\epsilon = \frac{1}{4}\sum_{i=i=1}^{n}\sum_{j=1}^{n} w_g(i) w_g(j) w(\alpha_i, \theta_j) f_a(\alpha_i, \theta_j) f_p(\alpha_i, \theta_j) \tag{14}$$

where $w_g(i)$ and $w_g(j)$ is the GGaussian weight corresponding to the Gaussian point x_i and x_j (corresponding to α_i and θ_j). . The constant 1/4 in front of the equations is due to the fact that the integral limit (0, 1) oof the dimensionless angle for eqs (6)–(8) is changed to (-1, 1) for the Gaussian quadrature.

3.2 Simulation Resuilts

Figure 10 and Figure 11 illustrrates the error analysis in computing the total and photo-peak efficiencies with different numbbers of Gaussian points in one angular direction, respectively. The true total efficiency and pphoto-peak efficiency is assumed to be one calculated with 200 Gaussian points in one angulaar direction (total of 40000 points). The results are calculated for a 2"x2" cylindrical NaI detetector with the γ-ray energy of 1 MeV. The tracer particle is 15 cm from the detector face and 1 15 cm from detector axis. For calculating the total efficiency (as well as solid angle), 10 Gauussian points (total 100 γ-rays) can yield a very good efficiency value with relative error less tthan 0.1%. However, for computing the photo-peak efficiency, large number of Gaussian poiints in one direction ($n \geq 30$) is required in order to obtain a good approximation to the truue efficiency value. As mentioned earlier, this is due to the fact that after γ-rays interact with t the detector crystal by Compton interaction, its new direction and travelled distance changes s randomly. In order to get a good statistical value, a relatively large number of Gaussian poinnts are needed.

Figures 12 and 13 show the e comparison of the present Monte Carlo simulation with other Monte Carlo simulation and e experimental measurements (Beam et al. 1978) of the total and photo-peak efficiencies. Th'he experimental data were obtained by placing a Cs-137 point source at various locations froom the detector face and axis, and measuring the total and photo-peak counts.

The total source intrinsic e efficiency and photo-peak efficiency are normalized with the efficiency for the particle locatating on the detector axis, respectively. When the angle with the detector axis increases, booth the source intrinsic efficiency and photo-peak efficiency increases as seen in Figs. 12 aand 13. The results from the present Monte Carlo simulation are very close to those from BBeam et al.'s (1978) Monte Carlo simulation. However, some differences between the Monte e Carlo simulation and experimental data exist. The reasons are provided by Beam et al. ((1978). When the distance between the detector and tracer particle increases, the differencces between the experimental data and the simulation decrease as illustrated in Fig. 14 (45 cmm from the center of detector face).

Attempts to reproduce the e results of Beam et al. (1978) have been made. The plots of the total intrinsic efficiency annd peak to total ratio as a function of γ-ray energy as shown in Figs. 15 and 16. These arure computed with the same parameters as used by Beam et al. (1978). The symbols in Figigs. 15 and 16 are the calculated efficiencies corresponding to different energy levels, and the e solid lines are curve fits to the simulated data. The simulation results shown in Figs. 15 and 1116 are very close to the results obtained by Beam et al. (1978).

The results of the Monte CCarlo simulation have also been compared with those of other Monte Carlo simulations (In aaddition to Beam et al.'s (1978) work). They all show good

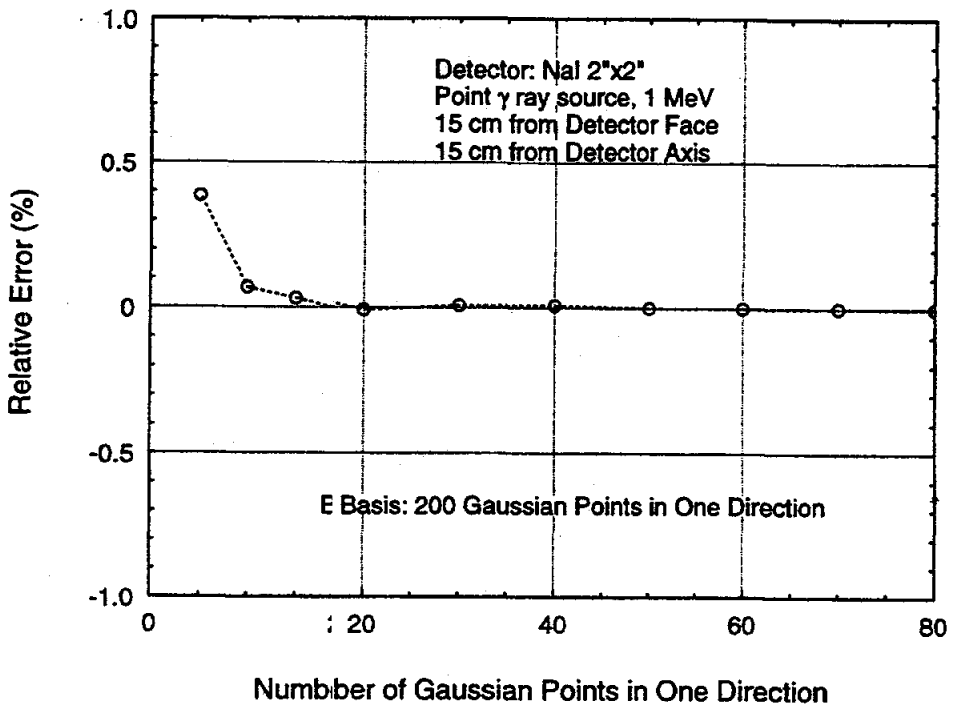

Figure 10: Error Analysis for (Calculating Detector Total Efficiency with Different Numbers of Gaussian Points

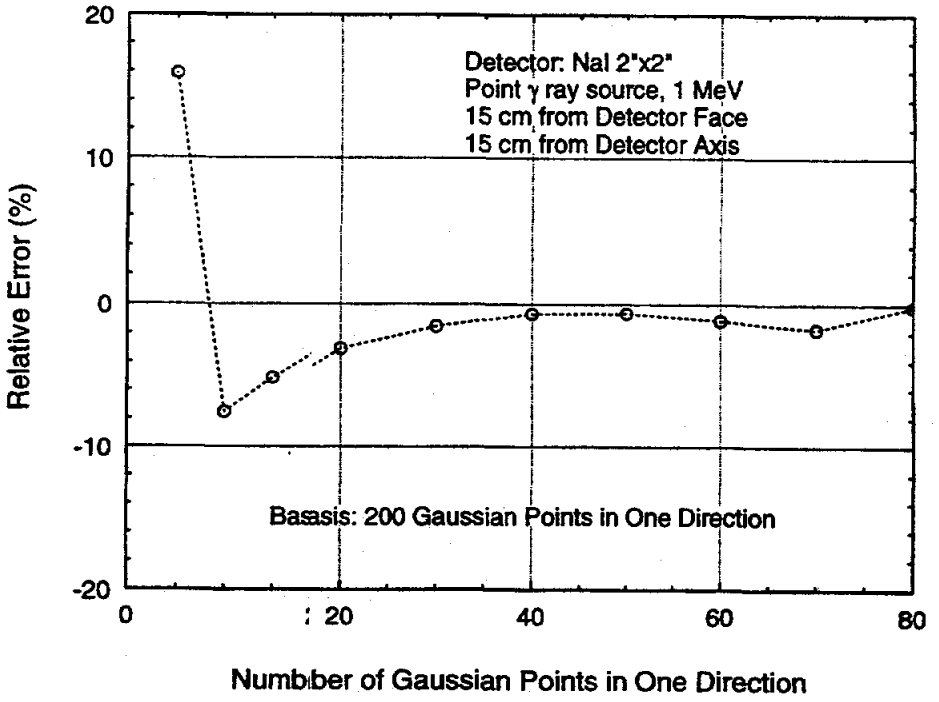

Figure 11: Error Analysis fonr Calculating Detector Photo-Peak Efficiency with Different Numbers of Gaussian Points

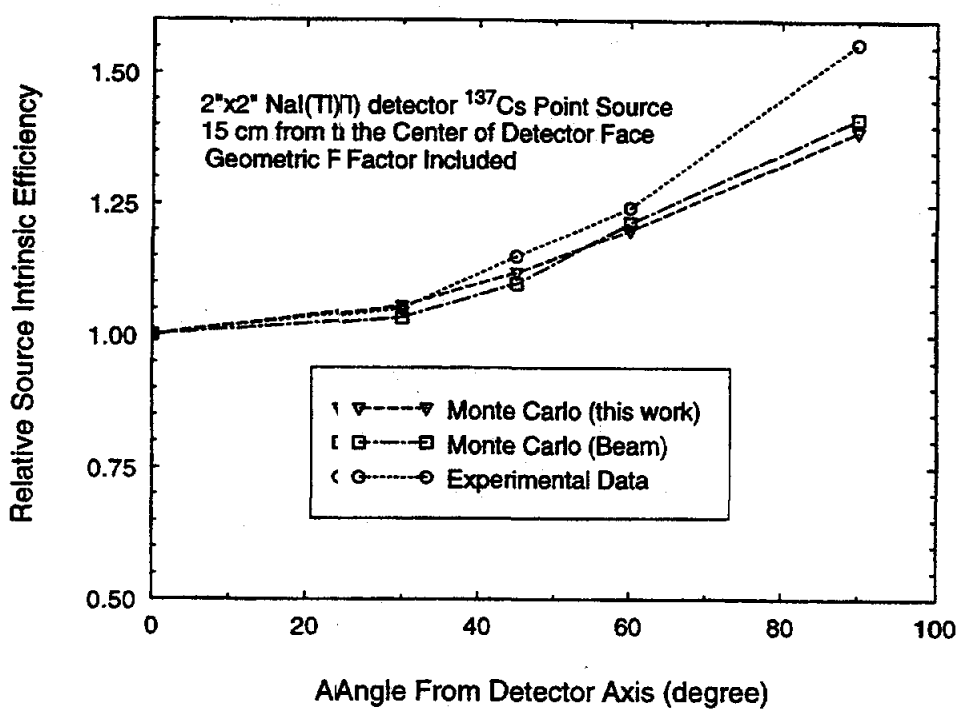

Figure 12: Companion of Presesent Monte Carlo Simulation with Other Simulation and Experimental Data on Total Efficiciency, 15 cm from the Center of Detector Face

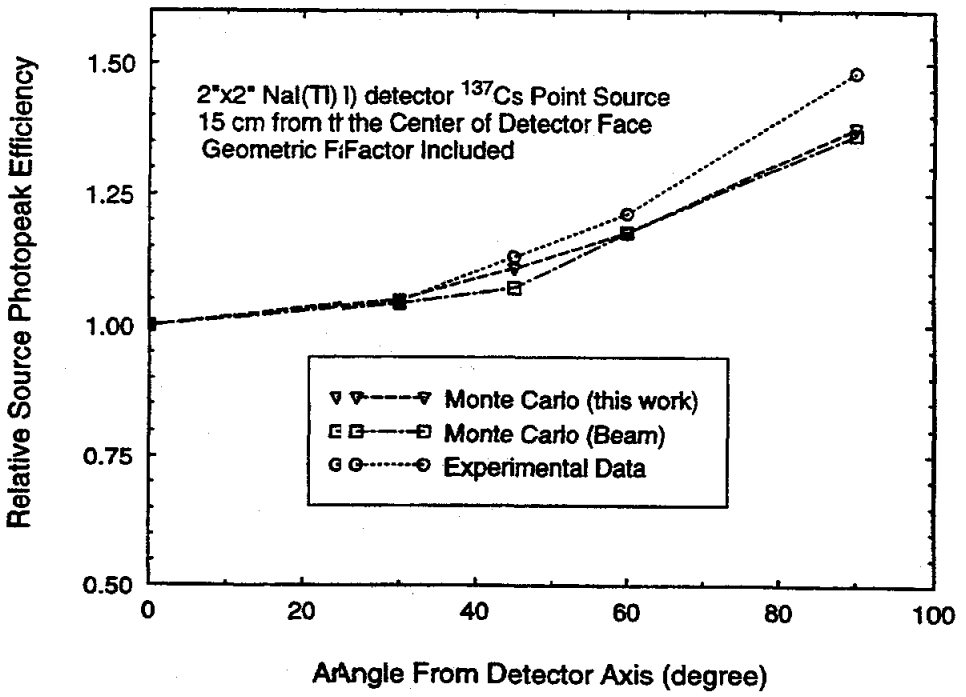

Figure 13: Comparison of Presesent Monte Carlo Simulation with Other Simulation and Experimental Data on Photo-Peaak Efficiency, 15 cm From the Center of Detector Face

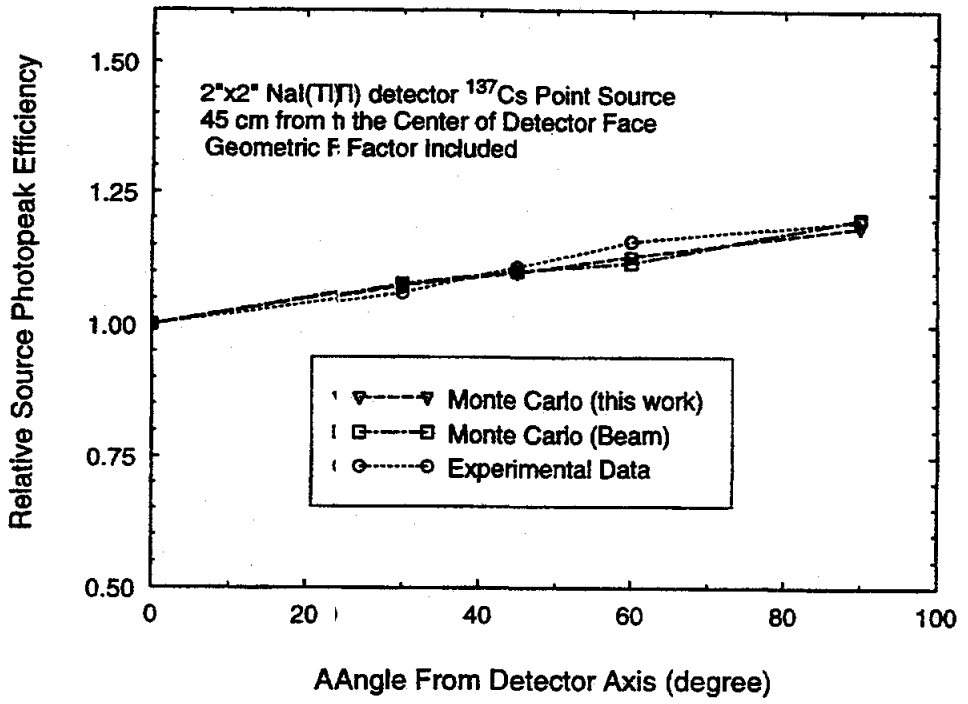

Figure 14: Comparison of Preesent Monte Carlo Simulation with Other Simulation and Experimental Data on Photo-Peæak Efficiency, 45 cm From the Center of Detector Face

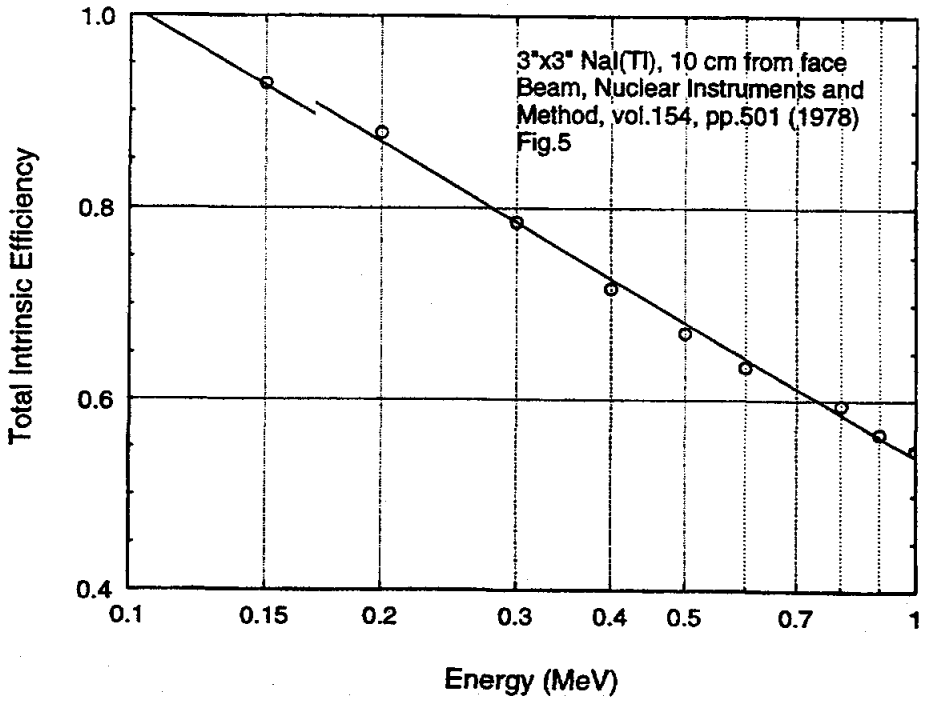

Figure 15: Total Intrinsic Effificiency as a Function of γ-ray Energy, 3"x3" NaI, 10 cm from Detector Face

agreement, and the present MMonte Carlo code is more efficient than the others (much less CPU time).

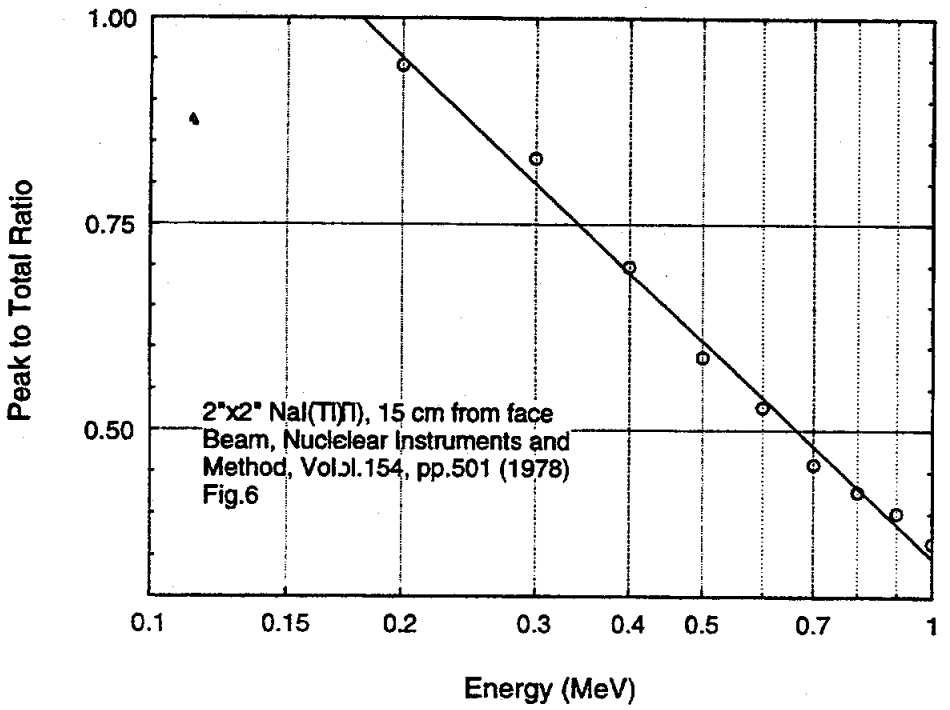

Figure 16: Photo-Peak Efficieency to Total Efficiency Ratio as a Function of γ-ray Energy, 2"x2" NaI, 15 cm from Detectctor Face

4 Verification of CARPT Velocity Data by Independent Methods

The second objective for the fifirst year of the project is to conduct studies in a single diameter column with the air-water r system and compare the results obtained at CREL using the CARPT-CT experimental commbination with the results obtained at OSU using Particle Image Velocimetry (PIV). The velocity measurements using CARPT were also to be compared with the results from heat pulslse anemometry.

PIV tests at identical conditions as those performed at CREL by CARPT are now in progress. Preliminary results s for the comparison between the velocity measurements by CARPT and those obtained ususing heat pulse anemometry at CREL are summarized here.

The Heat Pulse Anemometeter (HPA) uses a time-of-flow measurement technique to measure the mean liquid velocity bbetween two points in the flow field. It essentially measures the distribution of passage time of f the particles that start at one point in the flow and happen to meet at another second point ddownstream. Heat is used as tracer to tag the fluid particles. A

small heating element, the emnitter, is used to label the passing fluid elements. Downstream of this emitter a fast and sensisitive detector (hot film anemometer probe) registers the passage of the heated elements ofbf liquid. An impulse of heat tracer introduced at the emitter is therefore detected by the seensor probe similar to the case of a residence time distribution measurement.

In order to obtain sufficiemently large signal-to-noise ratios, tracer inputs in the form of pseudo-random sequences of s single pulses are used. The measured responses at the sensor which by themselves are meanningless, when cross correlated with the pseudo-random input pulse, yield an impulse responnse at the point of detection, called a time-of-flow distribution (see Figure 17). This responnse is interpreted by the following model which describes the

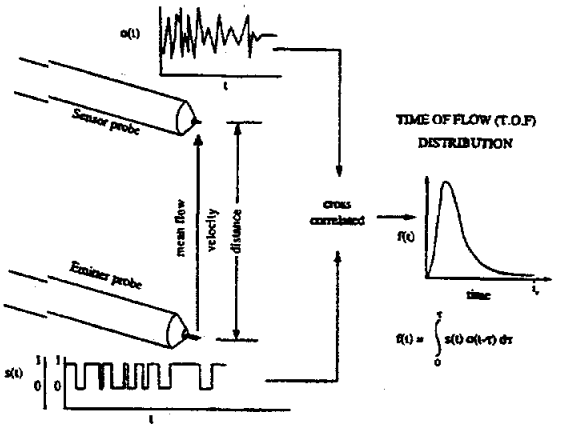

Figure 17: Schematic of HPA

mean flow of fluid particles beetween the emitter and the sensor by a Gaussian distribution function:

$$p(t) = \frac{c}{\sigma_0 t^\beta} \exp(-\frac{(t-\tau)^2}{2(\sigma_0 t^\beta)^2}) \tag{15}$$

where τ is the mean time-of-f-flow, σ_0 is the intensity of mixing and β denotes the type of mixing. Calculating τ fronm experimental measurements and knowing the distance of separation of the emitter fronm the detector, the mean velocity of the liquid between the emitter and sensor can be caldculated.

The variables during a meæasurement are the time of sweep, t_s, which is the time for one sweep during which several datata points are sampled, and the time of measurement, t_m, which is the total time for a given exexperimental measurement over which t_m/t_s number of sweeps are taken.

Table 3: Preliminary Reesults for Model Parameters from T.O.F. Measurements

U_G cm/s	t_s s	t_m s	τ s	σ_0 s	β
5	3.0	300	0.211	0.485	0.827
	2.0	"	0.234	0.493	0.762
	2.5	"	0.218	0.460	0.744
	2.5	2500	0.207	0.369	0.680
	2.5	3600	0.207	0.444	0.763
	2.5	5000	0.206	0.387	0.720
12	2.0	3500	0.124	0.218	0.496
	2.0	5000	0.126	0.349	0.651

Table 4: Comparison of Locaal Time Averaged Axial Velocities Using CARPT and HPA

U_G cm/s	CARPT cm/s	HPA (d/τ) cm/s
5	16.5	14.5
12	46.5	24.2, 23.8

Preliminary results have beeen obtained for experiments conducted in an 8″ column with the probes placed along the axiis of the column at a distance of 3 cm apart. The axial position of the emitter is 47 cm. The ı results for measurements at two gas velocities are presented. Table 3 shows the model parrameters at different values of t_m and t_s for each condition. The comparison of the calculilated mean axial liquid velocities with those from CARPT measurements are shown in Table 4. The comparison of the results at the lower gas velocity is reasonably good. However atat superficial gas velocity of 12 cm/s, the velocity obtained from HPA is quite lower than the CARPT measurements. At this high velocity it is possible that under the existing churn-turbuulent flow conditions, the variables of measurement mentioned above, along with the distancce between the emitter and sensor, may affect the measured signal and derived velocities ı from the heat pulse probe. Additional data collection and interpretation from HPA, and ı comparison with CARPT results are currently underway.

PIV is a technique based oon recording the images of particles used to seed the fluid for tracing the motion. The algoririthm essentially consists of image enhancement, identification of particle images, computatition of particle centroids, and computation of displacements between particle image pairs t to obtain the velocity and phase distribution. The gas-liquid flow in air-water bubble columnn of 10.54 cm (4") in diameter is considered for the comparison of the results from PIV and CCARPT. This column dimension is chosen due to the fact that PIV measurements for the liciquid phase velocity are more difficult to obtain in a larger diameter column. The time : averaged liquid phase velocities along a diametral plane of the column are to be obtaineed at superficial gas velocities of 2.0, 4.0 and 8.0 cm/s. The operating conditions chosen anre identical to the data available at CREL. The plane of the flow illuminated by the laser : sheet is 4 in. × 8 in. and approximately 3 mm thick. The comparison between the resultsts between PIV and CARPT will be provided in the next report. However, Figs. 18 and 19 demonstrate the results obtainable using PIV. Figure 18 shows the instantaneous velocity field of f the gas and liquid phase in a two dimensional bubble column 15 cm wide at a superficial gasis velocity of 1 cm/s. The time averaged velocity and Reynolds stress profiles for the same conditions are shown in Fig. 19.

5 Preparations ffor CARPT Runs on a High Pressure Bubble Columnn at Exxon

One of the key goals for this prroject is to conduct CARPT experiments in a high pressure air-water bubble column at Exxonn. In addition to CARPT, a number of related experiments such as pressure drop measurementsts, local holdup measurements as well as velocity measurements by heat pulse anemometry arre also being planned. The experiments are to be conducted in a 14.0 cm (6") diameter columnn approximately 240 cm (8 ft high). The flow behavior is to be studied over a range of preessures from 1 to 7 atmospheres.

A research team from CREEL has spent one week on Exxon campus in Florham Park, NJ, to plan on the CARPT experiinments for the study of a high pressure bubble column. Preliminary design for the hardware ccomponents required for setting up the CARPT system around the existing reactor setup at EExxon, and planning for the execution of the experiments were made during the visit. The deletector support structures have been designed to make use of the available column support : structure. Since it is for the first time that CARPT experiments are being conducted inin an opaque reactor, calibration of the system is anticipated to be a more tedious process : than usual. A positioning device that is capable of moving the tracer particle to various ı positions in the reactor, and such that its hardware does not hinder the radiation measuremment process, is being designed. Conceptually, the system is

planned on being completely aautomated so that the manual part of the calibration process is minimized. The isotopes too be used as tracers are Scandium-46 and Cobalt-60, each of approximately 350 to 450 micrrocuries activity for gas-liquid and slurry bubble columns, respectively. The experiments inin the high pressure bubble column at Exxon are planned on being accomplished in the sumnmer of 1997, somewhat earlier than originally suggested since this will provide more time to ɔ analyze the data during this grant.

6 References

Beam, G. B., L. Wielopolski, FR. P. Gardner, K. Verghese, 1978, Monte Carlo Calculation of Efficiencies of Right-circularrr Cylindrical NaI Detectors for Arbitrarily Located Point Sources, Nuclear Instruments a and Methods, 154, pp.501-508.

Coifman, R.; Wickerhauser, MA. V. 1992: Entropy-Based Algorithms for Best Basis Selection. IEEE Trans. on Inf.f. Theory, 38, 713-718

Daubechies, I. 1988: Orthonorrrmal Bases of Compactly Supported Wavelets. Comm. Pure Appl. Math. 41, 909-996

Hinze, J.O. 1959: Turbulence. . McGraw-Hill, New York

Larachi, F., Kennedy, G., and l Chaouki, J., 1994, A γ-ray Detection System for 3-D Particle Tracking in Multiphasıse Reactors, Nuclear Instruments and Methods in Physics Research, A338, 568-576.

Mallat, S; Zhong Z. 1992: Matıtching Pursuits with Time-Frequency Dictionaries. Preprint, New York University.

Menzel, T.; Weide, T.; Staudeccher, O.; Wein, O.; Onken, U. 1990: Reynolds Shear Stress for Modeling of Bubble Columnn Reactors. Ind. Eng. Chem. Res., 29, 988-994

Wickerhauser, M. V. 1994: Addapted Wavelet Analysis from Theory to Software. A. K. Peters, Wellesley, Massachusetttts.

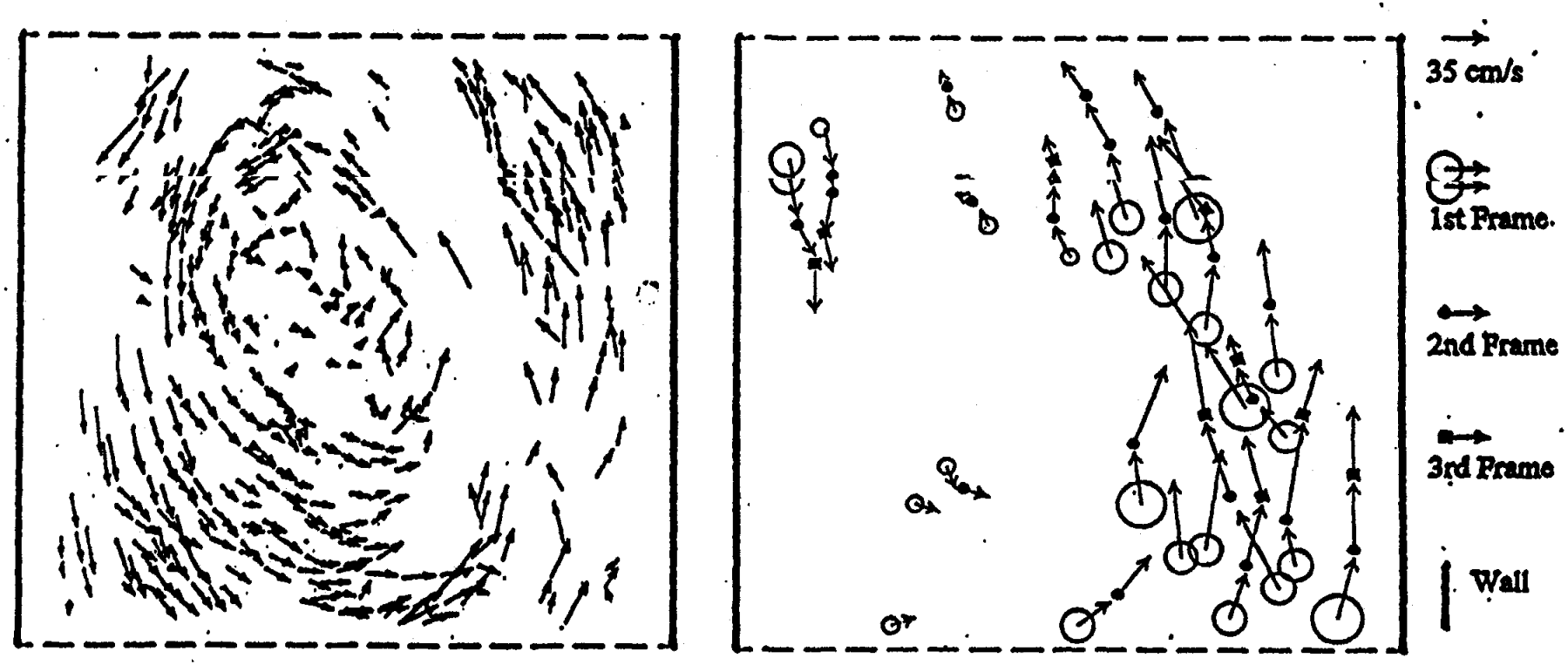

Figure 18: Sample PIV Result of the Liquid and Gas Velocity Fields in the 15 cm Column over 3 Consecutive Frames at a Superficial Gas Velocity of 1 cm/s

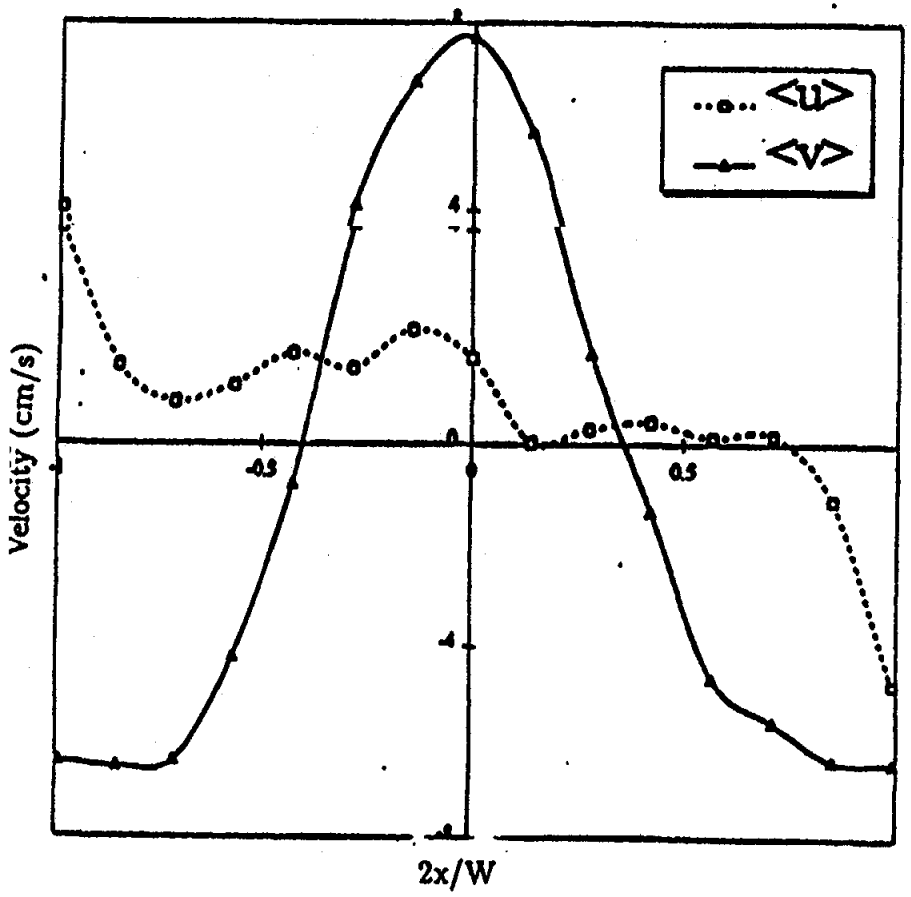

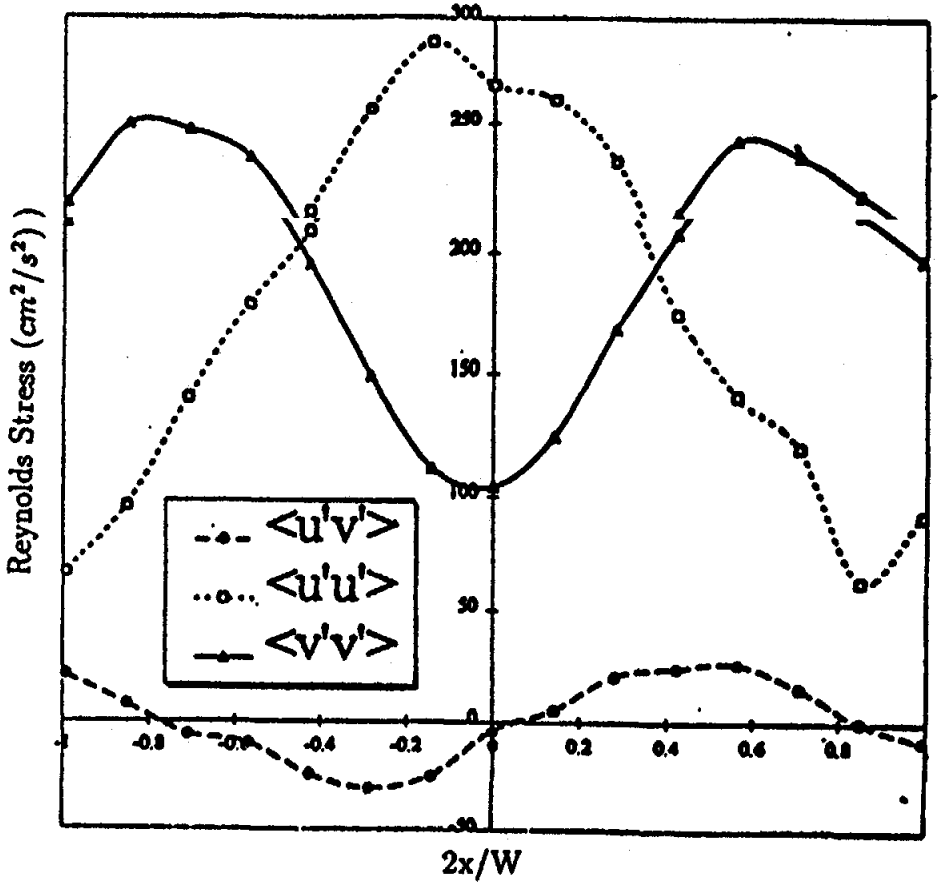

Figures 19: Radial Profiles of the Averaged Vertical and Horizontal Liquid Velocities and the Reynolds Stresses for the 15 cm Column (Gas Velocity = 1 cm/s Column over 3 Consecutive Frames at a Superficial Gas Velocity of 1 cm/s